UNIVERSIDADE FEDERAL DO RIO GRANDE DO SUL

PHYSICS POST GRADUATE PROGRAM

MASTER'S THESIS

Effect of dielectric discontinuity on a spherical polyelectrolyte brush: Molecular Dynamics simulations approach

(Estudo dos efeitos da descontinuidade dielétrica em uma "brush" de polieletrólitos esférica: Modelagem via Dinâmica Molecular)

Dissertação elaborada sob orientação do Prof. Dr. Alexandre Pereira dos Santos apresentada ao Instituto de Física da UFRGS como requisito final à obtenção do título de Mestre em Física.

Author: Vinicius Beltram Tergolina

Porto Alegre

2018

Abstract

In this work we present a molecular dynamics simulation of a polyelectrolyte spherical brush and counterions in a salt-free medium, in which the dielectric inhomogeneity between materials is taken in consideration. Polyelectrolyte brushes have been studied experimentally broadly, having shown a range of different applications such as for bioseparation and targeted drug/gene delivery. In spite of that, formal simulations and theories explaining its behavior are not as numerous. The theory and the work we present are unfold into more details throughout the thesis in the form of multiple sections, but the results remain contained to the paper annexed[1], published in 2017. We start with a brief introduction of the work and then present the paper, later on, the theory is further explored in the methodology appendix, and we finish with the final considerations for the work results and the project conclusion. The project consists of the aforementioned simulations with the main purpose of investigating the effect of the dielectric discontinuity, between the brush core and its surrounding medium, over the dynamics of the system. This is investigated through the use of the method of image charges. Properties of the polyelectrolyte brush are obtained for different parameters, including valence of the counterions, radius of the nanoparticle and the brush total charge. A mean-field theory is presented for the comparison with density profiles obtained for monovalent counterions, and we finish the paper by presenting the osmotic properties of the system.

Resumo

Neste trabalho apresentamos simulações em dinâmica molecular de uma "brush" de polieletrólitos esférica, cercada de contraíons, em um meio livre de sais, onde a heterogeneidade dielétrica entre os materiais é levada em consideração. Estes conjuntos de polieletrólitos tem sido estudados experimentalmente de maneira ampla, tendo mostrado uma gama de diferentes aplicações como o uso para biosseparação e como portadores de drogas/genes para transporte controlado. Entretanto, teorias e simulações formais que expliquem o seu comportamento não são tão numerosas. A teoria e o trabalho presentes são detalhados nesta dissertação na forma de múltiplas seções, mas os resultados permanecem contidos ao artigo anexado[1] publicado em 2017. Começamos com uma breve introdução do trabalho e então apresentamos o artigo, posteriormente a teoria é melhor explorada no apêndice da metodologia, finalmente, terminamos com as considerações finais para com os resultados do trabalho e as conclusões do projeto. O projeto consiste das simulações anteriormente mencionadas, as quais tinham o propósito principal de investigar os efeitos da descontinuidade dielétrica, entre o núcleo da "brush" e o meio em que está envolta, sobre a dinâmica do sistema. Isso é investigado através do uso do método de cargas imagem. As propriedades da "brush" de polieletrólitos também são obtidas para diferentes parâmetros, dentre os quais, a valência dos contra íons, o raio da nanopartícula central e a carga total da "brush". Uma teoria de campo médio é apresentada para comparação com os perfis de densidade obtidos para os contra íons monovalentes, e nós terminamos o artigo apresentando as propriedades osmóticas do sistema.

Content

1. Introduction

The study of polymer molecules and the development of theories appraising its dynamics is a fundamental benchmark of sciences in the twentieth century. Polymer molecules are present in our daily lives and the development of polymer-based technologies is important for an extensive range of applications, ranging from clothing and oil industries, to the medical sciences. Following the success of these applications, scientists have started to study these chain-like molecules in more complex structures, aiming to expand their usage. Among the mentioned structures this work focuses on polymer brushes.

In this work we refer to polymer chains as polyelectrolyte, as they are composed by charged monomers. Polyelectrolytes represent a broad class of materials that are abundant in biological systems. In addition, polyelectrolytes, being water soluble, are natural for aqueous environments and the two most studied of all biopolymers, DNA and RNA, are polyelectrolytes. A large class of synthetic polyelectrolytes exists as well, some of these are fundamental industrial chemicals. For example, polyacrylic acid is the key ingredient in diapers[2]. Despite the existence of a considerable interest in polyelectrolytes, and the theory of neutral polymer systems being well developed[3], polyelectrolytes remain one of the least understood subjects in the field of condensed matter.[4-7]

If long linear polyelectrolyte chains are grafted densely to a solid surface, an object known as a polyelectrolyte brush (PEB) results. The process usually involves the surface, coated with an initiator, being immersed in a monomer solution, this way the polymerization process result in a brush directly, alternatively, a solution of pre-synthetized polymers might be used as well[8]. As to the surface form, PEBs have been mainly studied as planar brushes, cylindrical brushes and spherical brushes. Therefore, polymer brushes can be classified as one-dimensional (1D), two-dimensional (2D), and three-dimensional (3D) brushes, corresponding to polymer chains grafted on polymer chains, planar surfaces, and spherical particles respectively (Fig. 1)[9]. Among these, the spherical geometry has been chosen for this work for its unique dielectric interface characteristics that will be presented later. In terms of chemical composition, polymer brushes can also be classified as homo-polymer brushes, when they are composed by solely one polymer type, mixed homo-polymer brushes, when they are composed by two or more polymer types side by side, and copolymer brushes, when they are composed by two or more polymers attached to each other. Here, for simplicity, we choose homo-polymer brushes.

The interest in the osmotic properties of polyelectrolyte multilayered materials such as PEB has been driven by the promise of the development of a novel class of biomaterials such as cell scaffold materials[10]. Depending on whether the constituent polyelectrolytes are pH sensitive or not, it was shown that the ion pairing density of the scaffold may be fine tuned by changes in pH or ionic strength, paramount for successful tissue regeneration. Related to PEB we can cite a novel amphiphilic pH-sensitive triblock polymer brush that was designed and synthesized successfully, resulting in their self-assembled polymeric micelles being used as hydrophobic anticancer drug delivery carriers to realize effectively controlled release[11]. These previously cited properties were of great motivation for this modelling project, and by performing a study on the dielectric inhomogeneity of a PEB-counterion system, we hope to better understand the PEB's behavior in a varying ionic strength solution against also varying brush conditions.

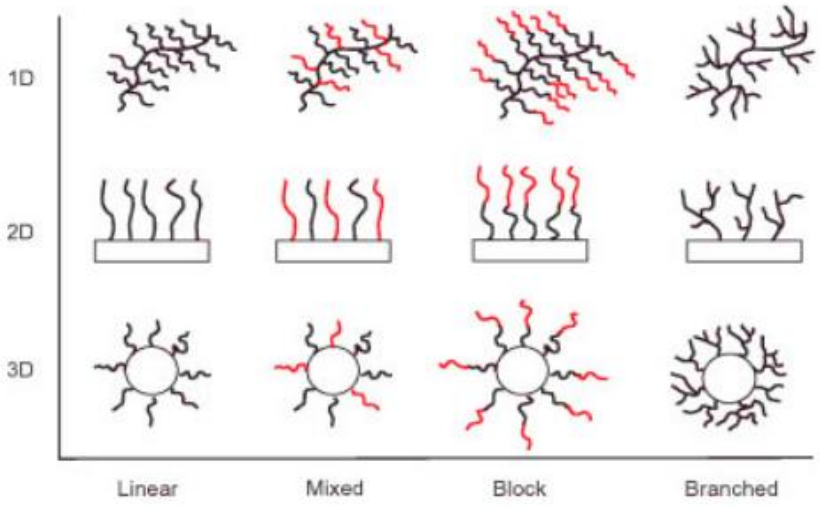

Figure 1

Possible brush configurations and geometries.

Traditionally, the problem of dielectric discontinuity has been treated by the method of image charges, which is inarguably the simplest one. Nonetheless, the real problem arises when we leave the planar geometry surfaces and enter the spherical geometry domains, for then the simple use of a punctual image charge for the calculation of the total electric potential produced by the surface polarization becomes insufficient. Across Section 2, we will explain a method developed by Levin and co-workers[12] based on a paper by Norris[13] that is able to deal with the calculations in an optimum manner. However, it is still worth remembering that the field is vast and other methods that will not be covered here, for reasons that are explained

ahead, are available since the subject was studied extensively in the past. Among these methods: Legendre polynomials,[14,15] and a variational formulation that is a more general method for the solution of the Poisson equatio[16,17]. The former is similar to the method utilized in this work, but has a big disadvantage in comparison to our choice. This will be further discussed later on.

Therefore, our simulation model is composed by a spherical core nanoparticle of colloidal dimensions with polyelectrolyte attached along its surface forming the spherical brush. The brush is immersed in a counterion solution that neutralizes the system charge depending on the number of monomers composing the polyelectrolytes. Everything lie inside a spherical cell. With this setup we hope to test the osmotic and dynamic properties of the brush and its surrounding solution, such as to better understand how the dielectric discontinuity affects the system against a number of parameters, *e.g.*, size of the nanoparticle, number of monomers per polyelectrolyte and ion valence.

Regarding colloids and polymers simulations, we had two choices for the brush modelling, Monte Carlo or Molecular Dynamics (MD) simulations; in consideration to the difficulty of applying the first to this subject, we choose the latter. This process involved utilizing the polymer bead-spring theory for the polyelectrolyte modelling, a hard spheres potential type for the volume exclusion of the solution, plus a stochastic and a friction term present on the final Langevin equation representing the Brownian motion. A simple Coulomb potential is utilized for the non-image electrostatic interactions while the most complex part of the simulations, the image charges originated from the dielectric inhomogeneity, are solved by the method previously cited that will be explained later. The theory section describes the mean field theory that is presented for comparison with the model results.

This dissertation is based on a paper published by us in 15 of September of 2017 in the Journal of Chemical Physics (showed in its entirety below). It will consist of the paper itself and a couple of annexes with the objective of further detailing the methodology used in the paper. The only results showed will be the ones present in the paper and, in the end, we will present a conclusion referring to new prospects and possibilities of the work discussed in the dissertation.

Effect of dielectric discontinuity on a spherical polyelectrolyte brush

Vinicius B. Tergolina, and Alexandre P. dos Santos

Citation: The Journal of Chemical Physics **147**, 114103 (2017); doi: 10.1063/1.5002526
View online: http://dx.doi.org/10.1063/1.5002526
View Table of Contents: http://aip.scitation.org/toc/jcp/147/11
Published by the American Institute of Physics

Effect of dielectric discontinuity on a spherical polyelectrolyte brush

Vinicius B. Tergolina[1] and Alexandre P. dos Santos[1,2,a)]
[1]*Instituto de Física, Universidade Federal do Rio Grande do Sul, Caixa Postal 15051, CEP 91501-970 Porto Alegre, RS, Brazil*
[2]*Fachbereich Physik, Freie Universität Berlin, 14195 Berlin, Germany*

(Received 16 May 2017; accepted 30 August 2017; published online 15 September 2017)

In this paper we perform molecular dynamics simulations of a spherical polyelectrolyte brush and counterions in a salt-free medium. The dielectric discontinuity on the grafted nanoparticle surface is taken into account by the method of image charges. Properties of the polyelectrolyte brush are obtained for different parameters, including valency of the counterions, radius of the nanoparticle, and the brush total charge. The monovalent counterions density profiles are obtained and compared with a simple mean-field theoretical approach. The theory allows us to obtain osmotic properties of the system. *Published by AIP Publishing.* [http://dx.doi.org/10.1063/1.5002526]

I. INTRODUCTION

The study of polyelectrolyte chains grafted to surfaces in a structure known as polyelectrolyte brush (PEB) has acquired substantial interest recently, as covered by many reviews.[1–7] With the development of experiments with DNA molecules outside of the intracellular environment, the study of cell-free gene expression has brought a new horizon for biotechnology. Examples go from double-stranded DNA brushes[8] to a single-step photolithographic biocompatible DNA mono-layer,[9] both on a biochip. In addition to these, it is also valid to refer to other applications for the synthesization of PEBs such as protein absorption,[10] bioseparation,[11] and targeted drug/gene delivery.[12] When referring to the term brush we assume that the grafting of the chains is dense enough in a way that the linear dimensions of the polyelectrolyte chains are much larger than the average distance between two neighboring charged polymers on the surface.[3] Previous studies[13–16] have shown that an essential property of a PEB is in its capability to confine a major quantity of counterions in a way to compensate its electrical charge, resulting in high osmotic pressure governing its stretching dynamics. Besides their extensive range of applications, PEBs have been studied in a range of different configurations as well, they can be generated either by grafting polyelectrolyte chains to planar[17–21] or to strongly curved systems as, for example, cylinders or spheres,[22–27] the last being the focus of our present work. Recently, different types of neutral polymer brushes with interesting properties composed by dipolar ions called zwitterions[28,29] in the form of polyzwitterions, have attracted attention and deserve citation.

In relation to spherical PEB, we can elicit their main structure as being formed by an inorganic core nanoparticle and an organic layer/shell in the form of polyelectrolyte chains grafted to its surface. As a result of their mechanical stability, high surface area, and ease of synthesis, silica/polymer hybrid nanoparticles have been studied more extensively.[11,30] Spherical PEBs also carry a number of advantages in comparison with planar ones. They can be studied by a wide variety of distinct methods coined for colloidal particles investigation, from scattering methods[31–34] to, more recently, dielectric spectroscopy.[35] Furthermore, the colloidal dimensions of the spherical PEB may be used to create well-defined surfaces of the order of many m^2 that can be used for nanoparticle/protein immobilization,[36,37] and they can also be viewed as models for the study of carboxylated latex particles that constitute a major industrial product.[38]

Amongst previous works, we can cite efforts to theoretically describe PEBs.[39–41] Regarding molecular dynamics (MD) simulations of spherical PEBs we can cite, as few examples, studies on the dependence of the brush thickness due to different parameters and conformations,[42–44] studies on brush size as a function of chain lengths, salt concentrations[45] and grafting densities—these accompanied by comparisons to mean field or self-consistent field theories.[46,47] The effect of multivalent ions on brush conformations was also extensively studied.[15,48–50] Nevertheless, MD simulations of PEBs that take into account the dielectric discontinuity between the grafted nanoparticle and surrounding medium are unprecedented so far, to the best of our knowledge. In spite of the preceding statement, the problem of charged particles in heterogeneous dielectric media has been broadly studied resulting in the coinage of different methods. Among those, we refer to treatments that can be applied in the spherical geometry for applications in colloidal science. Even if the computational cost is high, one can use Legendre polynomials[51,52] to perform MC or MD simulations. A variational formulation has gained attention lately as a more general method for the solution of the Poisson equation treating the local polarization charge density as a dynamic variable.[53,54] A more efficient method considers the images and uniformly distributed counter-image charges inside the dielectric void as an approximation that works very well for low dielectric constants.[55,56] In this work, we intend to include nanoparticle polarization using the previously mentioned method and perform MD simulations of a PEB in a salt-free suspension. In addition, a simple Poisson-Boltzmann

a)Electronic mail: alexandre.pereira@ufrgs.br

(PB) theory is presented in order to account for the counterions concentration in mean-field regime.

In Sec. II, we explain the model and simulation method followed by the presentation of the theory developed for weak electrostatic coupling. The results are presented in the subsequent section. In the last section we finish describing the conclusions of the present work and general perspectives.

II. MODEL AND SIMULATION METHOD

We follow a standard coarse-grained model for the polymer chains and counterions confined in a spherical cell of radius R. The $N_p = 14$ chains are represented by N_m charged hard spheres (monomers) of radii $r_m = 2$ Å and charge $+q$, where q is the proton charge. The first monomers of the chains are grafted to the surface of a sphere of radius a and relative dielectric constant ϵ_c, representing the nanoparticle base particle. The first monomers are all uniformly distributed on the nanoparticle surface, grafted at distance r_m from it. The N_c counterions are modeled as hard spheres with effective radii $r_c = r_m$ and charge $-\alpha q$, where α is the valency. The number of counterions is defined as $N_c = N_p N_m/\alpha$ in order to keep the system with zero total charge. The medium in which the polyelectrolyte is immersed is represented by structureless water with relative dielectric constant $\epsilon_w = 80$. The Bjerrum length, defined as $\lambda_B = q^2/\epsilon_w k_b T$, is 7.2 Å, the value for water at room temperature.

Following a method previously developed,[55] we investigate the influence of the nanoparticle polarization by means of image charges. The calculation of image charges for the spherical geometry is not as straightforward as for the planar geometry. The continuity of the tangential component of the electric field and of the normal component of the displacement field across the nanoparticle-water interface, requirements of the Maxwell equations boundary conditions, give rise to a counter-image line charge in addition to the punctual image charge that is the usual requirement for planar geometry.[57] The electrostatic potential at an arbitrary position $\mathbf{r}$ produced by the arbitrary charge q_i located at $\mathbf{r}_i$ outside the nanoparticle is approximated by

$$\phi(\mathbf{r};\mathbf{r}_i) = \frac{q_i}{\epsilon_w|\mathbf{r}-\mathbf{r}_i|} + \frac{\gamma q_i a}{\epsilon_w r_i|\mathbf{r}-\frac{a^2}{r_i^2}\mathbf{r}_i|} + \frac{\gamma q_i}{\epsilon_w a}\log \times\left(\frac{rr_i - \mathbf{r}\cdot\mathbf{r}_i}{a^2 - \mathbf{r}\cdot\mathbf{r}_i + \sqrt{a^4 - 2a^2(\mathbf{r}\cdot\mathbf{r}_i) + r^2 r_i^2}}\right), \quad (1)$$

where $r_i = |\mathbf{r}_i|$, $r = |\mathbf{r}|$, and $\gamma = (\epsilon_w - \epsilon_c)/(\epsilon_w + \epsilon_c)$. This expression is valid[55] for $\epsilon_w \gg \epsilon_c$. The total electrostatic energy is

$$U_{elec} = \sum_{i=1}^{N-1}\sum_{j=i+1}^{N} q_j\phi(\mathbf{r}_j;\mathbf{r}_i) + \sum_{i=1}^{N}\frac{\gamma q_i^2 a}{2\epsilon_w(r_i^2 - a^2)} + \sum_{i=1}^{N}\frac{\gamma q_i^2 \log(1-\frac{a^2}{r_i^2})}{2\epsilon_w a}. \quad (2)$$

The two last terms above are the ionic electrostatic self-energy.

The elastic bonds between adjacent monomers of the same chain in the brush are modeled by the following nonlinear energy potential,[58–61]

$$U_{bond} = \sum_{ad.mon.}\frac{A}{2}(r - r_0)^2, \quad (3)$$

where $r = |\mathbf{r}_i - \mathbf{r}_j|$ is the distance between adjacent monomers i and j. The sum is made over all adjacent monomers of the same polymer chains, $A = 0.9k_BT$ and $r_0 = 5$ Å, following the aforementioned Ref. 61.

The total force acting on the charged specie k is

$$\mathbf{F}_k = -\nabla_{\mathbf{r}_k}(U_{elec} + U_{bond}). \quad (4)$$

The molecular dynamics simulations were performed for constant time steps by means of a well-known Langevin equation,[62]

$$\mathbf{p}_i'(t) = \mathbf{F}_i(t) - \Gamma\mathbf{p}_i(t) + \mathbf{R}_i(t), \quad (5)$$

where $\mathbf{p}_i(t)$ is the momentum of particle i at time t, $\mathbf{F}_i(t)$ is the force felt by this particle, Γ is the friction coefficient, and $\mathbf{R}_i(t)$ is the stochastic force acting on particle i, which satisfy the fluctuation dissipation relation. The Verlet-like method developed by Ermak[62] is used to solve the previous equation.

The mechanism chosen to avoid the superposition between all particles and surfaces is a hard sphere potential. This was preferred over a caped Lennard-Jones type potential for the reason that the latter was tested showing little to no difference from the hard spheres potential while requiring time steps much smaller to advert simulation crashes. In Fig. 1, a snapshot of MD simulations after equilibrium is shown for monovalent counterions.

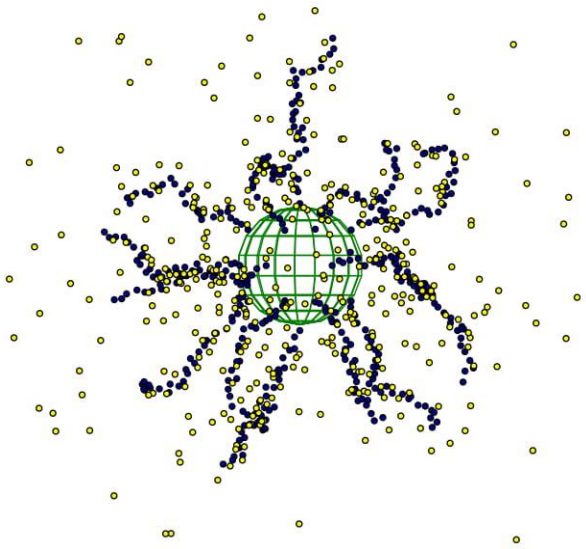

FIG. 1. Representation of the spherical PEB. Darker spheres represent monomers, while lighter spheres represent counterions.

III. THEORY

At room temperature, electrostatic correlations between monovalent ions can be neglected.[63] A mean-field PB equation is used to obtain the density profile of counterions. We do not consider the dielectric discontinuity on the nanoparticle-water interface because this effect is very small in this regime, as it will be shown in the Results section. Also, the qualitative

results obtained with the present method allow us to consider this approximation. However, it is important to mention that this effect can be important when more accuracy is necessary in the study of the electric double layer.[55,56]

The charge distribution of PEB is constructed as if all the monomers are aligned with the nanoparticle center, with effective distance between them equals to $r_{ef} = 0.75 r_m$ to account for the bending of the chains. The modified PB equation takes the form

$$\nabla^2\phi(r) = -\frac{4\pi}{\epsilon_w}\left[\sum_{i=1}^{N_m}\sigma_i\delta(r-r_i) - q\alpha\rho(r)\right], \tag{6}$$

where $\phi(r)$ is the mean electrostatic potential, σ_i are the charge densities of the corresponding layers of monomers, given by $\sigma_i = N_p/4\pi r_i^2$, where $r_i = a + r_m + (i-1)2r_{ef}$. The counterions density profile is given by

$$\rho(r) = N_c \frac{e^{-\beta\alpha q\phi(r)}}{4\pi\int_{(a+r_c)}^{R} dr' r'^2 e^{-\beta\alpha q\phi(r')}}. \tag{7}$$

The solution of Eq. (6) is performed by Picard iterative process.

IV. RESULTS

The results are presented in the form of average particles concentration profiles and average effective PEB radius (the distance between the center of the grafted nanoparticle and the more distant monomer), see Fig. 2. We start by studying the effect of the dielectric discontinuity on the counterion distribution around the PEB, see Fig. 3. We choose the following values for the nanoparticle relative dielectric constant, $\epsilon_c = 2$ and $\epsilon_c = \epsilon_w$. Whereas in the first choice we choose the typical dielectric constant value of silica, in the second case, we ignore the dielectric discontinuity by having the nanoparticle represented by the same material as the medium in which it is inserted, water. Silica nanospheres coated with polymer brushes have already been used for effective separation of glycoproteins.[11]

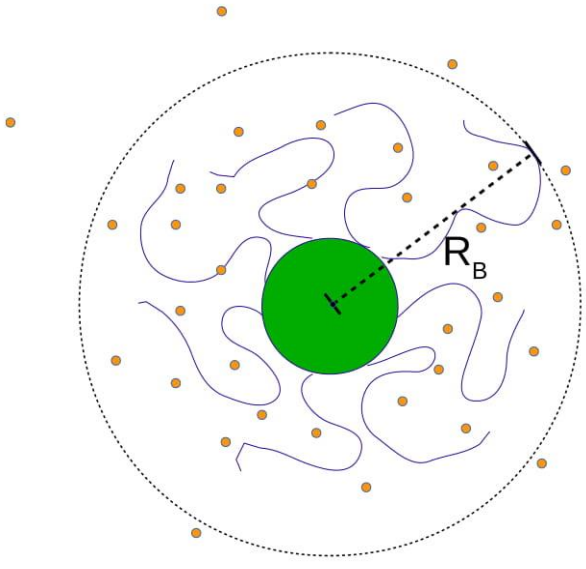

FIG. 2. Definition of effective PEB radius, R_B.

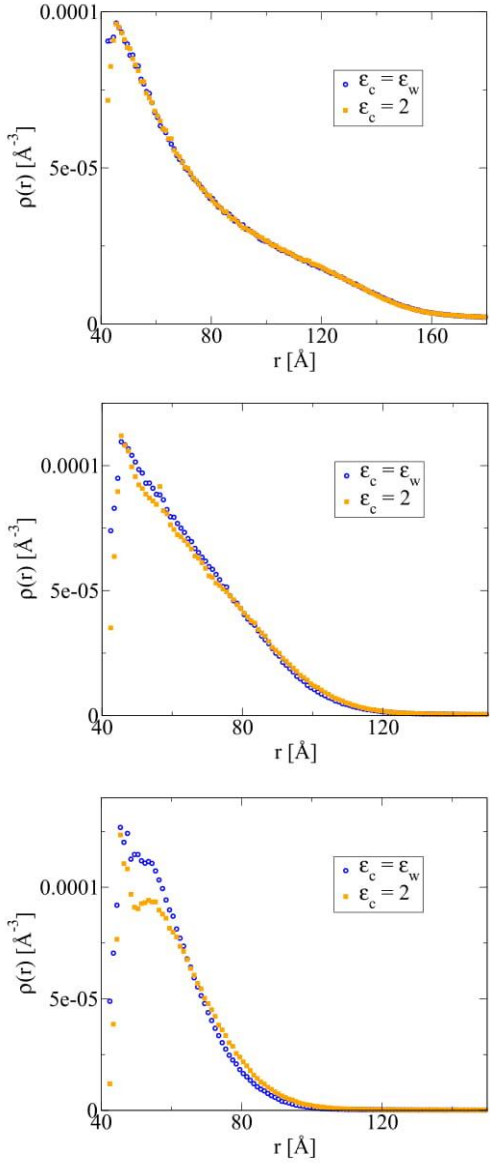

FIG. 3. Density profiles of counterions obtained for $\alpha = 1, 2, 3$, from top to bottom, respectively. Polyelectrolyte brush individual chains with $N_m = 30$ and nanoparticle radius $a = 40$ Å.

The influence of the dielectric discontinuity on monovalent ions is very small and most of the pattern we see is caused by osmotic pressure inside the brush, which tends to repel counterions. Similar brush configuration has been extensively explored before without consideration for dielectric discontinuity so that the results showing that multivalent counterions are more deeply absorbed are expected. Although the density maximum concur for both distributions of multivalent ions, we find that the polarization of the silica nanoparticle tends to broaden their distributions since they feel more repelled by their image charges. Also, the effective brush radius, R_B, tends to be higher due to image charges of chains, which can affect the ionic distribution far away from brush. For charged nanoparticles and surfaces, the consequence of a dielectric discontinuity in ionic distribution is very local, near surfaces.[54–56,64] The importance of the polarization effect for the trivalent case can also be observed in the density profiles of monomers, see Fig. 4.

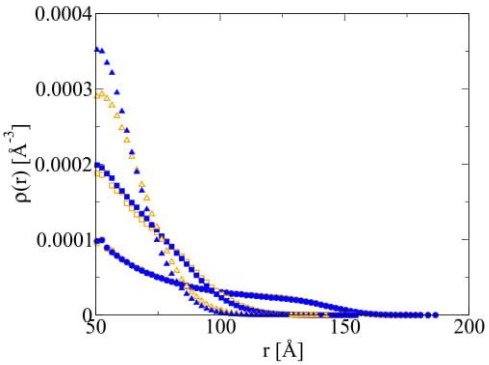

FIG. 4. Density profiles of monomers obtained for $\alpha = 1, 2, 3$, circles, squares, and triangles, respectively. Full symbols represent $\epsilon_c = \epsilon_w$, while open symbols $\epsilon_c = 2$. The parameters are the same as in Fig. 3.

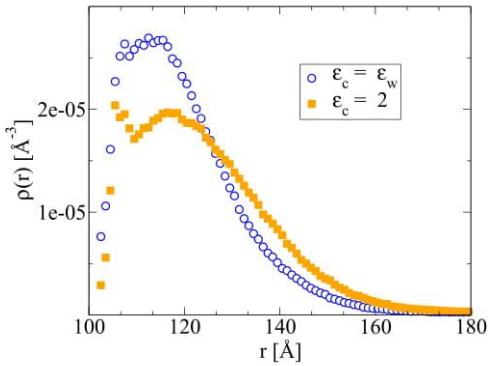

FIG. 6. Density profiles of counterions obtained for $\alpha = 3$ for two relative dielectric constants of the nanoparticle. Polyelectrolyte brush individual chains with $N_m = 30$ and grafted nanoparticle radius $a = 100$ Å.

Moving further, we study the brush behavior over different number of monomers and different counterion valence by calculating R_B, see Fig. 5. We define the PEB radius, R_B, as the average distance between the center of grafted nanoparticle and the more distant monomer. Here we confirm that image charges have little to no influence over the brush diameter for monovalent counterions. This is not the case for larger brushes composed by 30 and, more explicitly, 42 monomers, surrounded by multivalent ions. In this case we can find a considerable increase in R_B when accounting for the dielectric discontinuity when compared with the homogeneous case. The polyelectrolyte chain total charge is high for a sufficient number of monomers and they are, by construction, near the nanoparticle surface. This means that image charges play an important role in the brush radius value when this value is sufficiently small. The difference in both approximations can achieve ≈9% for the discussed parameters. The smaller values obtained for R_B in the case of multivalent ions are in agreement with experiments that relate the collapse of the spherical PEB with the addition of multivalent ions in solution.[15,65]

The density profile for a special case in which the brush's nanoparticle is relatively big ($a = 100$ Å) is shown in Fig. 6. The polarization of the nanoparticle undoubtedly has a strong influence over the trivalent counterions profile, showing that the role played by nanoparticle polarization is not only to further fend the colloid and the counterions but also to spread

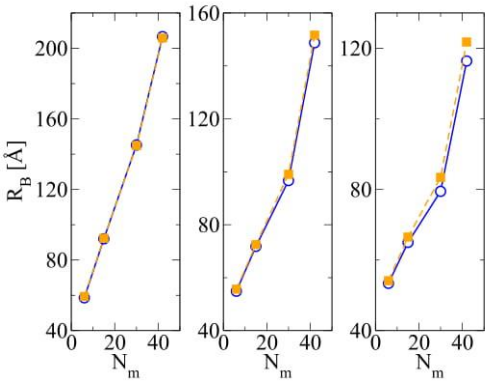

FIG. 5. PEB average effective radius as a function of N_m for $a = 40$ Å and $\alpha = 1, 2, 3$, from left to right panels, respectively. The circles represent the case, which $\epsilon_c = \epsilon_w$, while squares, $\epsilon_c = 2$.

their distribution, in comparison with the unpolarized nanoparticle. It is also worthy to remark the double peak pattern present in the $\epsilon_c = 2$ curve, much more protruding than in the $\epsilon_c = \epsilon_w$ curve, indicating two clear preferred regions for the trivalent counterions. This is a competition between the electrostatic interaction of multivalent ions with the entire brush and with their local chain, see also Fig. 3, bottom panel. The polarization of the nanoparticle separates more explicitly these regions as a result of the shifting of the ionic distribution.

In order to measure the effect of nanoparticle polarization on counterions distributions as a function of nanoparticle curvature, we calculate the relative difference between profiles defined as $\Delta = \frac{\sqrt{\int_a^R dr[\rho_2(r) - \rho_{\epsilon_w}(r)]^2}}{\int_a^R dr\,\rho_{\epsilon_w}(r)}$, where $\rho_{\epsilon_w}(r)$ is the counterion profile for $\epsilon_c = \epsilon_w$ and $\rho_2(r)$ for $\epsilon_c = 2$. We take the cases of Fig. 3 and similar ones except for the parameters $a = 80$ Å and $R = 500$ Å for comparison. We set these lengths in order to maintain constant volume fraction in the comparison. The volume fraction is defined as $\phi_{frac} = a^3/R^3$. For $\alpha = 1$, we obtain for Δ the values 0.0041 and 0.0032. For divalent $\alpha = 2$ sets, we obtain 0.0115 and 0.0166. The values found for $\alpha = 3$ were 0.0265 and 0.0252, all numbers for $a = 40$ Å and $a = 80$ Å, respectively. These results show us that there is no influence of the nanoparticle curvature in the polarization effect on the counterions distribution for constant PEBs volume fraction. However, if we take for comparison two sets with the same cell radius R but with different nanoparticles radius a, the curvature can decrease the effect of dielectric discontinuity on the counterions distribution. We take the trivalent case of Fig. 3 and the set of Fig. 6. The parameters are the same with the exception of the nanoparticle radius, which is 40 Å and 100 Å, respectively. We then obtain the values 0.0265 and 0.0424, respectively, for the relative difference of the profiles, showing that the decrease in curvature enhances the aforementioned effect.

We move further in the results section by comparing simulations with the present theory for monovalent ions, see Fig. 7. The theory is not able to describe properly the monovalent counterions structure around the brush, except for shorter chains. However, the agreement is very good in the region far from nanoparticle surface, for the studied chain lengths. The

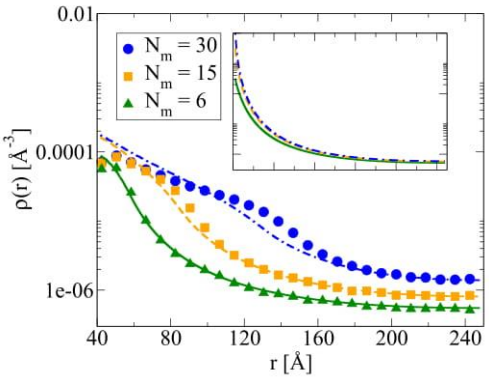

FIG. 7. Density profiles of counterions obtained for $\alpha = 1$, $a = 40$ Å and various number of monomers, N_m. The lines represent the results of the present theory, while symbols represent the results of simulations. The inset shows the solutions of PB equation if all the charged monomers are located on the nanoparticle surface, for the same parameters and the same x and y axis scales.

present method allows us to quantitatively account the adsorption of monovalent counterions, which means that osmotic properties of a brush suspension can be studied using the present method. We can define, for example, effective charges of PEBs, as the subject for a future work. It is important to mention the interesting effect that the boundary ionic concentrations are not saturated with the increase in the macroparticle charge as it is observed in colloidal suspensions; see the inset of Fig. 7. This saturation observed in colloidal suspensions reflects the independence of the colloidal effective charge with the colloidal charge.[66,67] This is not the case for PEBs as can be seen in Fig. 7. For multivalent counterions, as expected, the theory is not able to describe the asymptotic curve, as can be seen in Fig. 8, not even by reasonably decreasing the value of r_{ef}. The counterion-counterion and counterion-monomer electrostatic correlations take place and the present mean-field theory is not able to account for these effects.

As an application of the method for monovalent counterions, we calculate the osmotic coefficient, which is defined as the fraction between the pressure and ideal pressure given by $\phi_{osm} = \rho_{bulk}/\rho_{id}$, where ρ_{bulk} is the counterion bulk concentration and $\rho_{id} = N_c/V$, where V is the volume accessible to the N_c counterions.[68] In Fig. 9, we show the curves of ϕ_{osm} versus ϕ_{frac} for the same parameters as in Fig. 7 obtained with the

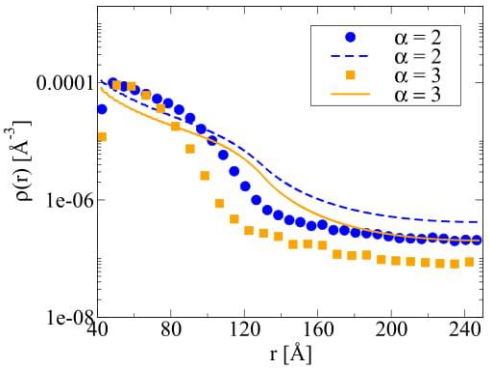

FIG. 8. Density profiles of multivalent counterions obtained for $N_m = 30$ and $a = 40$ Å. The lines represent the results of the present theory, while symbols represent the results of simulations.

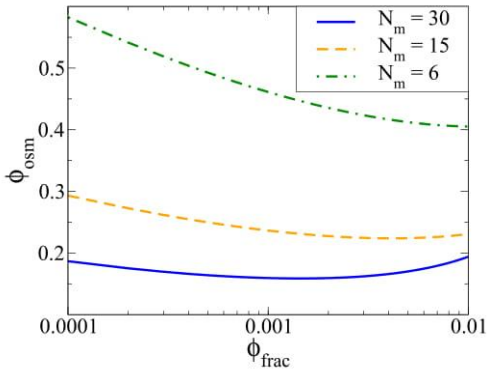

FIG. 9. Osmotic coefficient versus volume fraction for the same parameters of Fig. 7.

present theory. For longer chains, we can observe a minimum in the curve. Also, by increasing the length of grafted chains we obtain a smaller osmotic coefficient that is in agreement with experimental measurements.[68]

V. CONCLUSIONS

In this work we have performed MD simulations of a spherical polyelectrolyte brush in a salt-free solution. The dielectric discontinuity in the grafted nanoparticle surface is taken into account. We observe that for monovalent counterions at room temperature, the grafted nanoparticle polarization is not mandatory to describe the ionic structure around the brush. Also, the effective polyelectrolyte brush radius is not very affected for the studied parameters apart from the cases with trivalent counterions and longer chains, in which, the differences can achieve $\approx 9\%$. Furthermore, in these cases, the concentration profiles of counterions and monomers are considerably different comparing both approximations. We also present a mean-field Poisson-Boltzmann theory for low electrostatic coupling regime. This method allows us to obtain quantitatively the asymptotic counterionic concentration, leading us to calculate the osmotic coefficients of PEBs suspensions. The effective charges of brushes are going to be studied in a future work. We have observed that the nanoparticle curvature influences the polarization effect for constant cell radii. In this comparison the volume available to counterions is in practice the same. However, if we keep the PEB's volume fraction constant in the comparison, the effect of the curvature is negligible. In this comparsion the volume available to counterions is very different. This suggests that the effect of the polarization depends also on the ionic strength of the solution.

ACKNOWLEDGMENTS

This work was partially supported by the CNPq, CAPES, and Alexander von Humboldt Foundation.

[1]S. Minko, Polym. Rev. **46**, 397 (2006).
[2]M. Ballauff and O. Borisov, Curr. Opin. Colloid Interface Sci. **11**, 316 (2006).
[3]M. Ballauff, Prog. Polym. Sci. **32**, 1135 (2007).
[4]P. Jain, G. L. Baker, and M. L. Bruening, Annu. Rev. Anal. Chem. **2**, 387 (2009).
[5]K. Binder and A. Milchev, J. Polym. Sci., Part B: Polym. Phys. **50**, 1515 (2012).

[6]I. Szilagyi, G. Trefalt, A. Tiraferri, P. Maroni, and M. Borkovec, Soft Matter **10**, 2479 (2014).
[7]S. Das, M. Banik, G. Chen, S. Sinha, and R. Mukherjee, Soft Matter **11**, 8550 (2015).
[8]E. Karzbrun, A. M. Tayar, V. Noireaux, and R. H. Bar-Ziv, Science **345**, 829 (2014).
[9]A. Buxboim, S. S. Daube, and R. Bar-Ziv, Mol. Syst. Biol. **4**, 181 (2008).
[10]S. J. Sofia, V. Premnath, and E. W. Merrill, Macromolecules **31**, 5059 (1998).
[11]L. D. Jiang, H. Bagan, T. Kamra, T. C. Zhou, and L. Ye, J. Mater. Chem. B **4**, 3247 (2016).
[12]A. Wittemann, T. Azzam, and A. Eisenberg, Langmuir **23**, 2224 (2007).
[13]P. Pincus, Macromolecules **24**, 2912 (1991).
[14]O. V. Borisov, T. M. Birshtein, and E. B. Zhulina, J. Phys. II **1**, 521 (1991).
[15]Y. Mei, K. Lauterbach, M. Hoffmann, O. V. Borisov, M. Ballauff, and A. Jusufi, Phys. Rev. Lett. **97**, 158301 (2006).
[16]Y. Mei, M. Hoffmann, M. Ballauff, and A. Jusufi, Phys. Rev. E **77**, 031805 (2008).
[17]H. Ahrens, S. Forster, and C. A. Helm, Macromolecules **30**, 8447 (1997).
[18]M. Biesalski and J. Ruhe, Macromolecules **32**, 2309 (1999).
[19]E. P. K. Currie, A. B. Sieval, M. Avena, H. Zuilhof, E. J. R. Sudholter, and M. A. C. Stuart, Langmuir **15**, 7116 (1999).
[20]J. Ruhe, M. Ballauff, M. Biesalski, P. Dziezok, F. Grohn, D. Johannsmann, N. Houbenov, N. Hugenberg, R. Konradi, S. Minko, M. Motornov, R. R. Netz, M. Schmidt, C. Seidel, M. Stamm, T. Stephan, D. Usov, and H. Zhang, Adv. Polym. Sci. **165**, 79 (2004).
[21]D. Bendejacq, V. Ponsinet, and M. Joanicot, Eur. Phys. J. E **13**, 3 (2004).
[22]L. F. Zhang, K. Yu, and A. Eisenberg, Science **272**, 1777 (1996).
[23]C. Biver, R. Hariharan, J. Mays, and W. B. Russel, Macromolecules **30**, 1787 (1997).
[24]P. Guenoun, F. Muller, M. Delsanti, L. Auvray, Y. J. Chen, J. W. Mays, and M. Tirrell, Phys. Rev. Lett. **81**, 3872 (1998).
[25]R. Hariharan, C. Biver, J. Mays, and W. B. Russel, Macromolecules **31**, 7506 (1998).
[26]X. Guo, A. Weiss, and M. Ballauff, Macromolecules **32**, 6043 (1999).
[27]F. Muller, P. Fontaine, M. Delsanti, L. Belloni, J. Yang, Y. J. Chen, J. W. Mays, P. Lesieur, M. Tirrell, and P. Guenoun, Eur. Phys. J. E **6**, 109 (2001).
[28]M. Chen, W. H. Briscoe, S. P. Armes, H. Cohen, and J. Klein, Eur. Polym. J. **47**, 511 (2011).
[29]M. Kobayashi, Y. Terayama, M. Kikuchi, and A. Takahara, Soft Matter **9**, 5138 (2013).
[30]I. Ab Rahman and V. Padavettan, J. Nanomater. **2012**, 132424 (2012).
[31]W. Groenewegen, A. Lapp, S. U. Egelhaaf, and J. R. C. van der Maarel, Macromolecules **33**, 4080 (2000).
[32]X. Guo and M. Ballauff, Phys. Rev. E **64**, 051406 (2001).
[33]N. Dingenouts, M. Patel, S. Rosenfeldt, D. Pontoni, T. Narayanan, and M. Ballauff, Macromolecules **37**, 8152 (2004).
[34]E. Schneck, E. Papp-Szabo, B. E. Quinn, O. V. Konovalov, T. J. Beveridge, D. A. Pink, and M. Tanaka, J. R. Soc., Interface **6**, S671 (2009).
[35]X. X. Guo and K. S. Zhao, J. Phys.: Condens. Matter **29**, 055102 (2017).
[36]A. Wittemann, B. Haupt, and M. Ballauff, Phys. Chem. Chem. Phys. **5**, 1671 (2003).
[37]G. Sharma and M. Ballauff, Macromol. Rapid Commun. **25**, 547 (2004).
[38]D. Distler, *Waessrige Polymerdispersionen* (Wiley-VCH, New York, 1999).
[39]Y. Rakita, D. Golodnitsky, and A. Natan, J. Electrochem. Soc. **161**, E3049 (2014).
[40]A. Erbas and M. O. de la Cruz, Macromolecules **49**, 9026 (2016).
[41]A. Naji, R. R. Netz, and C. Seidel, Eur. Phys. J. E **12**, 223 (2003).
[42]F. S. Csajka and C. Seidel, Macromolecules **33**, 2728 (2000).
[43]C. Seidel, Macromolecules **36**, 2536 (2003).
[44]D. J. Sandberg, J. M. Y. Carrillo, and A. V. Dobrynin, Langmuir **23**, 12716 (2007).
[45]N. A. Kumar and C. Seidel, Macromolecules **38**, 9341 (2005).
[46]S. Z. He, H. Merlitz, L. Chen, J. U. Sommer, and C. X. Wn, Macromolecules **43**, 7845 (2010).
[47]H. Merlitz, C. W. Li, C. X. Wu, and J. U. Sommer, Soft Matter **11**, 5688 (2015).
[48]W. D. Tian and Y. Q. Ma, J. Phys. Chem. B **113**, 13161 (2009).
[49]L. T. Yan, Y. Y. Xu, M. Ballauff, and A. H. E. M. A. Boker, J. Phys. Chem. B **113**, 5104 (2009).
[50]L. Liu, P. A. Pincus, and C. Hyeon, Macromolecules **50**, 1579 (2017).
[51]R. Messina, J. Chem. Phys. **117**, 11062 (2002).
[52]G. I. Guerrero-García and M. O. de la Cruz, J. Phys. Chem. B **118**, 8854 (2014).
[53]V. Jadhao, F. J. Solis, and M. O. de la Cruz, Phys. Rev. Lett. **109**, 223905 (2012).
[54]V. Jadhao, F. J. Solis, and M. O. de la Cruz, J. Chem. Phys. **138**, 054119 (2013).
[55]A. P. dos Santos, A. Bakhshandeh, and Y. Levin, J. Chem. Phys. **135**, 044124 (2011).
[56]A. Bakhshandeh, A. P. dos Santos, and Y. Levin, Phys. Rev. Lett. **107**, 107801 (2011).
[57]W. T. Norris, IEE Proc.: Sci., Meas. Technol. **142**, 142 (1995).
[58]R. S. Dias, A. A. C. C. Pais, P. Linse, M. G. Miguel, and B. Lindman, J. Phys. Chem. B **109**, 11781 (2005).
[59]M. Quesada-Perez and A. Martín-Molina, Soft Matter **9**, 7086 (2013).
[60]G. Luque-Caballero, A. Martín-Molina, and M. Quesada-Perez, J. Chem. Phys. **140**, 174701 (2014).
[61]A. P. dos Santos, M. Girotto, and Y. Levin, J. Phys. Chem. B **120**, 10387 (2016).
[62]M. P. Allen and D. J. Tildesley, *Computer Simulations of Liquids* (Oxford University Press, Oxford, New York, 1987).
[63]Y. Levin, Rep. Prog. Phys. **65**, 1577 (2002).
[64]A. P. dos Santos and Y. Levin, J. Chem. Phys. **142**, 194104 (2015).
[65]F. A. Plamper, A. Walther, A. H. E. Muller, and M. Ballauff, Nano Lett. **7**, 167 (2007).
[66]S. Alexander, P. M. Chaikin, P. Grant, G. J. Morales, and P. Pincus, J. Chem. Phys. **80**, 5776 (1984).
[67]E. Trizac, L. Bocquet, M. Aubouy, and H. von Grunberg, Langmuir **19**, 4027 (2003).
[68]B. Das, X. Guo, and M. Ballauff, Prog. Colloid Polym. Sci. **121**, 34 (2002).

2. Methodology Appendix

In this section, we further explain the methodology applied in the paper, which has not been discussed in detail in the original publication.

2.1 Polymer Model

When we consider a real polymers molecule with covalent bonds linking its monomers it is known that the conformational states that characterize this molecule are susceptible to entropic barriers imposed by the interaction of individual monomers with each other. These conditions that limit the range of configurations that can be assumed by a molecule are explained by a range of effects, among which is the correlation of bound angles. To overcome this we use the concept of an ideal chain. By applying the work of De Gennes[18] we rely on the concept of scale to fulfil the mentioned condition. Consequently, our model monomers, that will compose each of the polymer arms in the brush model, have to represent hundreds or thousands of real monomers in each model monomer to fulfil this scale conditions.

By analyzing the polymer arm at longer distances all its torsion and bond angles become equally probable, this enables us to treat the polymer arms as freely jointed chains. The best and most utilized method to model this type of polymer arms is the bead-spring model. In this model springs are used to represent chemical bonds and beads to represent monomers, see Fig. 2, thus we had to choose a proper energy potential to represent the spring[19]:

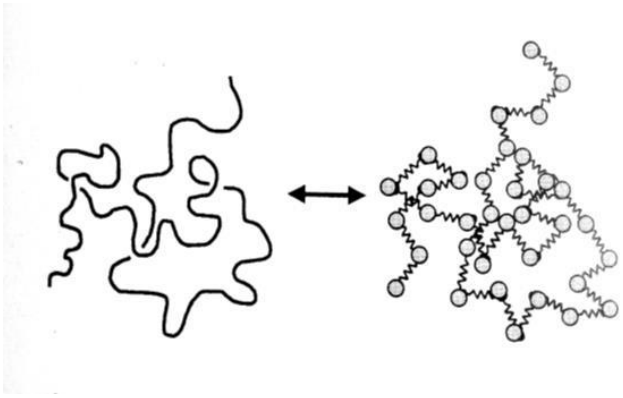

Figure 2

The bead-spring model is used to represent real polymer chains.

$$U_{bond} = \sum_{ad.mon.} \frac{A}{2} |\boldsymbol{r} - \boldsymbol{r_0}|^2 \ , \qquad (1)$$

where $\boldsymbol{r} = |\boldsymbol{r_i} - \boldsymbol{r_j}|$ is the distance between adjacent monomers i and j. The sum is made over all adjacent monomers of the same polymer chains, A = $0.9k_B$T and $r_0 = 5\dot{A}$. We choose this non-linear potential to better represent the elastic nature of the spring representing the bonds, in contrast with the harmonic oscillator, where the elasticity is represented by a linear equation. From this, we can easily calculate the elastic force acting over adjacent monomers of the same chain by taking Eq. (1) position derivative.

2.2 Image Charges in a Dielectric Sphere

The idea of an electric image charge in a conducting sphere was introduced by Kelvin and developed by Maxwell[20] and Jeans[21]. The method of image charges is considered the main solution to the problem of a single charge, placed inside or outside a spherical/planar boundary between two materials of different dielectric constant, when combined with fields due to the charges induced on the boundary. The spherical and planar geometries have the advantage of disposing of exact analytical methods for the problem's solution whereas more complex geometries may rely only on numerical solutions.

The first to calculate the analytic solution for the image magnitude was Norris[22], he considered a source charge placed outside a spherical boundary of radius a with different dielectric constants inside and outside the sphere (ϵ_i and ϵ_0 respectively). Starting from Maxwell's boundary conditions: fields parallel to the interface (either side) are equal, and the field normal to the inner face is ϵ_i/ϵ_0 times that on the outer face, expressing the fact that the electric displacement is continuous across the boundary. He expressed the fields due to the source charge and the surface charges as a series of Legendre polynomials and matched the fields associated with each Legendre polynomials at the surface. He then showed that the fields due to the surface charge can be expressed as due to image charges as described in Fig. 3. In the case of an external source charge Q, the field outside the sphere created by the charges induced on the surface of the sphere is equal to the field generated by a point image inside the sphere Q' at the inversion point, $\boldsymbol{r'_i} = \boldsymbol{r_i}a^2/{r_i}^2$, and a distributed charge that stretches from the inversion point to the center $\lambda(r)$. The magnitude of the image punctual charge is equal (but of opposite sign) to the total charge in the distributed part, so that the sphere as a whole appears neutral.

The distributed image charge (counterimage), its potential and the potential generated by the point image charge are described by Eq. (2), (3) and (4) respectively:

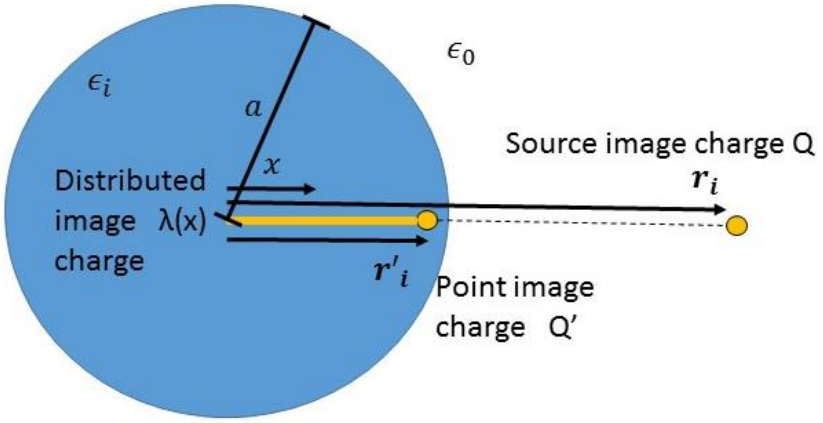

Figure 3

Explanation of the image charge composition for the spherical geometry.

$$\lambda(x) = -\frac{Q\prime(1+\gamma)}{2r_i}\left(\frac{x}{r_i'}\right)^{\frac{\gamma-2}{2}}, \tag{2}$$

$$\phi_{ci}(\boldsymbol{r};\boldsymbol{r_i}) = \frac{a^2}{\epsilon_0 r_i}\int_0^1 d\zeta \frac{\lambda\left(\zeta\frac{a^2}{r_i}\right)}{\left|\boldsymbol{r}-\zeta\frac{a^2}{{r_i}^2}\boldsymbol{r_i}\right|}, \tag{3}$$

$$\phi_{im}(\boldsymbol{r};\boldsymbol{r_i}) = \frac{Q\prime}{\epsilon_0\left|\boldsymbol{r}-\frac{a^2}{{r_i}^2}\boldsymbol{r_i}\right|}, \tag{4}$$

here, r_i is the charge distance, the magnitude of the point image charge is $Q' = \gamma Q a/r_i$ where $Q = \alpha q$ is the source charge given by the valence α times the elementary charge q, and $\gamma = (\epsilon_0 - \epsilon_i)/(\epsilon_0 + \epsilon_i)$.

Following this work, it was shown[23] that the integration on Eq. (3) (which cannot be performed exactly) can be simplified by considering that the dielectric constant inside the boundary is much smaller than the dielectric constant of the surrounding medium. Fortunately, this is the case for colloids where the dielectric constant of the colloid (usually silica) is much smaller than the dielectric constant of its surrounding medium (usually water). This

leads to $\gamma \approx 1$, and in this case, the counterimage charge is uniformly distributed $\bar{\lambda}(x) = -Q'/r'_i$, and the mentioned integral can be performed exactly resulting in the exact potential for the counterimage:

$$\bar{\phi}_{ci}(\boldsymbol{r};\boldsymbol{r_i}) = \frac{Q}{\epsilon_0 a} log\left(\frac{rr_i - \boldsymbol{r}.\boldsymbol{r_i}}{a^2 - \boldsymbol{r}.\boldsymbol{r_i} + \sqrt{a^4 - 2a^2(\boldsymbol{r}.\boldsymbol{r_i}) + r^2 {r_i}^2}}\right), \quad (5)$$

where the over-bar is used to denote the uniform line-charge approximation. The ion self-counterimage interaction potential when $\boldsymbol{r} = \boldsymbol{r_i}$ reduces to a simpler equation:

$$\bar{\phi}_{ci}^{\,self}(\boldsymbol{r};\boldsymbol{r_i}) = \frac{Q}{\epsilon_0 a} log\left(1 - \frac{a^2}{r_i^2}\right) \quad (6)$$

Both this expressions were imperative for the development of our simulations as they allowed us to obtain the force over the polymer-ion system due to the dielectric inhomogeneity between the colloid, the central piece of the polyelectrolyte brush, and the surrounding medium.

2.3 Polyelectrolyte Brush Model

After explaining the theories behind our simulation, we can now explain how they assemble to form the Langevin equation, which is the core equation for the calculation of the steps in the Brownian-dynamics simulation. Our configuration is illustrated by Fig. 4 (also present in our paper).

The polyelectrolyte brush is composed by a central colloid nanoparticle with 14 charged polymers chains tethered to it. The number of counterions was varied as to neutralize the charge of the 14 polymers. The number of monomers composing each polymer was variable but they were always monovalent whereas the counterions could have higher valences. The total energy of the system includes the spring interaction between monomers described in section 2.1, the electrostatic interactions described by: the colloid surface polarization effect of section 2.2, and a simple Coulomb potential. Despite that the self counterimage potential Eq. (6), which only applies to the charged particle that generates it, the counterimage potential Eq. (5) of each charged particle applies to all particles. This makes simulations including the dielectric inhomogeneity effect more costly in computational time.

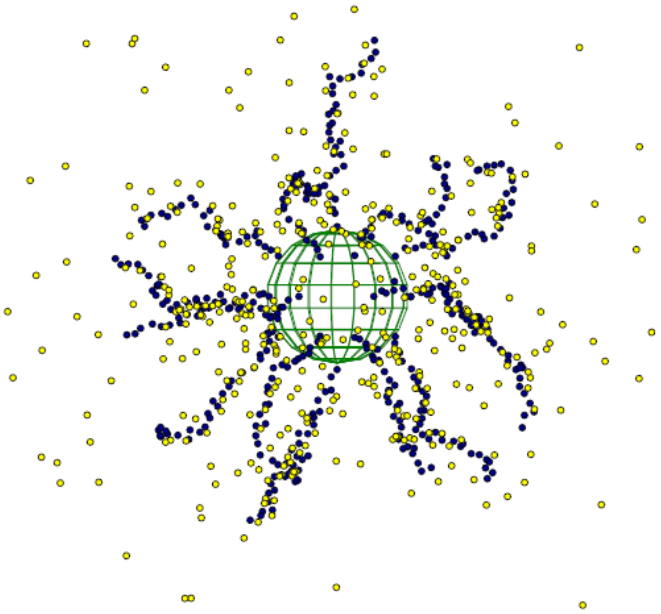

Figure 4

Snapshot of the simulation representing the model.

The total electrostatic potential that applies for all particles is:

$$\phi(\boldsymbol{r};\boldsymbol{r_i}) = \frac{Q}{\epsilon_0|\boldsymbol{r}-\boldsymbol{r_i}|} + \phi_{im}(\boldsymbol{r};\boldsymbol{r_i}) + \gamma\bar{\phi}_{ci}(\boldsymbol{r};\boldsymbol{r_i}) \ , \tag{7}$$

here the first term accounts for the Coulomb interaction between particles, the second and the third terms refer to the image and counterimage charges potentials, respectively. In the third term, it is used the condition of charge neutrality to correct the ion-counterimage interaction from Eq. (5) by including a prefactor γ. This, then, is the Green function for the present geometry. Therefore, the total electrostatic energy for a system of N particles is given by:

$$U_{elec} = \sum_{i=1}^{N-1}\sum_{j=i+1}^{N} q_j\phi(\boldsymbol{r_j};\boldsymbol{r_i}) + \sum_{i=1}^{N} U_i^{self}, \tag{8}$$

$$U_i^{self} = \frac{\gamma Q^2 a}{2\epsilon_0(r_i^2 - a^2)} + \frac{\gamma Q\bar{\phi}_{ci}^{\ self}(\boldsymbol{r_i})}{2}, \tag{9}$$

where U_i^{self} is the interaction energy of the ion i with its own image and counterimage charges.

Eq. (8) represents the total interaction energy of the counterions, the monomers of the polymer chains have their interaction energy represented by Eq. (8) plus Eq. (1), the elastic bond energy. The energies by specific specimen (monomer or counterion) have their negative derivative taken for each of the tri-dimensional Cartesian coordinate $\mathbf{F_{ion}} = -\nabla_{r_{ion}}(U_{elec})$ or $\mathbf{F_{monomer}} = -\nabla_{r_{monomer}}(U_{elec} + U_{bond})$ resulting in the total interaction force over an individual specimen. The Brownian-dynamics forces will be discussed in the next session.

2.4 Numerical Solution of the Model

After obtaining the interaction force on each of the individual particle of the system we can assemble a generalized Langevin equation to describe their motion on each of the MD simulation steps:

$$m\dot{v}_i(t) = F_i(t) - \zeta_i v_i(t) + R_i(t) \tag{10}$$

The equation describes the acceleration $\dot{v}_i(t)$ of a particle i with mass m_i, under a force $F_i(t)$, friction coefficient ζ_i and stochastic force $R_i(t)$. The friction here is present to maintain the temperature of the system constant. Following Einstein relation, $R_i(t)$ has to respect the relation $\langle R_i(t)R_j(t')\rangle = 2\zeta_i k_B T_0 \delta_{ij}\delta(t-t')$ [24].

In Eq. (10), a constant temperature consistent with the canonical ensemble is maintained by balancing the dissipative effect of the frictional terms with a stochastic force due to thermal noise. Consequently, we utilized this constant temperature thermal bath condition in our simulations, allowing us to rely on a well-known numerical method to solve Eq. (10). We employ a velocity Verlet method that follows a standard protocol for solving non-linear differential equations of the type given by Eq. (10). The equations of motion from this can be obtained by integrating the following expressions over the interval $(t, t+\Delta t)$ [25].

$$x(t+\Delta\mathrm{t}) = x(t) + c_1 v(t)\Delta\mathrm{t} + c_2 \frac{F(t)}{m}\Delta t^2 + \delta r^G, \tag{11}$$

$$v(t+\Delta t) = c_0 v(t) + (c_1 - c_2)\frac{F(t)}{m}\Delta t + c_2 \frac{F(t+\Delta t)}{m}\Delta t + \delta v^G, \quad (12)$$

where:

$$c_0 = e^{-\zeta \Delta t}, \quad (13)$$

$$c_1 = (\zeta \Delta t)^{-1}(1 - c_0), \quad (14)$$

$$c_2 = (\zeta \Delta t)^{-1}(1 - c_1), \quad (15)$$

$$c_3 = (\zeta \Delta t)^{-1}\left(\frac{1}{2} - c_2\right). \quad (16)$$

In these equations, the stochastic integrals of $R_i(t)$ are δr^G and δv^G, are sampled from a bivariate Gaussian distribution of zero mean:

$$\delta v_{i\alpha} = \sigma_v \left(c_{rv}\eta_1 + \sqrt{(1 - c_{rv}^2)}\right)\eta_2 , \quad (17)$$

$$\delta r_{i\alpha} = \sigma_r \eta_1 , \quad (18)$$

$${\sigma_r}^2 = \langle(\delta r_{i\alpha}^G)\rangle = \frac{k_B T}{m}\frac{1}{\zeta \Delta t}\left[2 - \frac{1}{\zeta \Delta t}(3 - 4e^{-\zeta \Delta t} + e^{-2\zeta \Delta t})\right], \quad (19)$$

$${\sigma_v}^2 = \langle(\delta v_{i\alpha}^G)\rangle = \frac{k_B T}{m}\left(1 - e^{-2\zeta \Delta t}\right) , \quad (20)$$

$$c_{rv} = \Delta t \frac{k_B T}{m}\frac{1}{\sigma_v \sigma_r}\frac{1}{\zeta \Delta t}\left(1 - e^{-\zeta \Delta t}\right)^2 , \quad (21)$$

here ${\sigma_r}^2$and ${\sigma_v}^2$ are the variances of δr^G and δv^G and c_{rv} their correlation coefficient. η_1 and η_2 are two independent random numbers with Gaussian

distribution of zero average and unit variance, easily obtainable by the use of specific functions of any programming language library.

Finally, by applying the mentioned equations we were able to develop an algorithm that solved Eqs. (11,12) for each time step Δt of our simulation for each Cartesian coordinate (x, y, z), separately, resulting in a precise description of the system for x(t), y(t), z(t), $v_x(t)$, $v_y(t)$, $v_z(t)$ for every Δt. This algorithm also included a particle overlap prevention mechanism in the form of a hard-sphere potential, plus appropriate spherical reflections on the cell inner and outer boundaries. It is important to state that by dividing all measures of - position, particle radius, cell size - by the Bjerrum length $\lambda_B = \beta q^2/\epsilon_0 = 7.2\,\dot{A}$, we are able to work with only dimensionless quantities, allowing us to drop k_B, T, m and q (we work only with the valence α) from the equations. This way we have only r_m, the monomer radius, r_c the counterion radius, a the colloid radius, N_m the number of monomers, N_c the number of counterions, α the counterions charge valence, γ, ζ and Δt as the input parameters of our algorithm. This allowed us to tune the system parameters in the search for interesting conditions in our study.

2.5 Poisson-Boltzmann Equation

The Poisson-Boltzmann (PB) equation describes a model for when a charged surface comes in contact with an ionic solution. It is of great practical and theoretical importance. The PB equation is the most widely used equation[26] that describes the distribution of electrical potential involved in the interaction between colloids, polymers and the ionic solution. The Poisson equation for the electrostatic potential of the counterions in the solution is described by: $\nabla^2\Phi = \frac{-4\pi\rho}{\epsilon_0}$, where ρ is the charge density and Φ the electrostatic potential.

Our model has to include the charged monomers in this equation, their position is described in Fig. 4, there we have 14 polymers spread through the colloid's surface, one on each pole and 12 spaced throughout the body. In order to mathematically express this we use the Dirac delta function representing each of the 14 polymers and their individual monomers. Therefore the Poisson equation for the system is expressed by:

$$\nabla^2\Phi(r) = \frac{-4\pi q}{\epsilon}\left[\sum_{i=1}^{N_m}\sigma_i\delta(r-r_i) - \alpha\rho(r)\right], \qquad (22)$$

here σ_i are the charge densities of the corresponding layers of monomers given by $\sigma_i = N_p/4\pi r_i^2$, N_p being the number of polymers, $r_i = a + r_m + (i-1)2r_{ef}$, representing the distance of each monomer shell to the center of the coordinate system as a sum of the colloid radius a, the monomer radius r_m and $r_{ef} = 0.75\, r_m$, to account for bending of the chains. $\rho(r)$ is the local

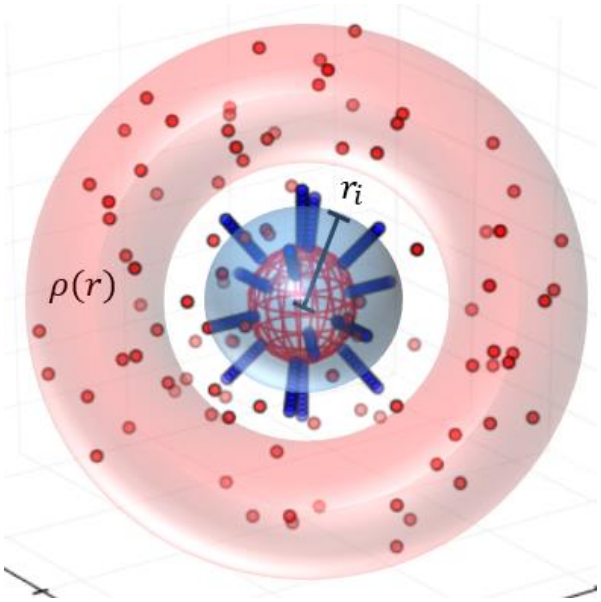

Figure 5

Graphical representation of the PB-Equation setup.

density of counterions at a distance r from the center of the system (Fig. 5), this is given by the Boltzmann distribution. We use a mean field approximation setting the potential of mean force as the mean electrostatic potential of all ions, finishing with the PB equation:

$$\rho(r) = N_c \frac{e^{-\beta\alpha q\Phi(r)}}{4\pi \int dr' r'^2 e^{-\beta\alpha q\Phi(r')}} , \qquad (23)$$

where β is the inverse of the Boltzmann constant times the temperature of the system. The bottom part of Eq. (23) is calculated over the limits of the colloid and the boundary of the spherical cell.

This is an approximation, which is expected to work only when the correlations between counterions is small. The reason for that is in the mean

field approximation we use, we do not account ions positional correlations in opposition to the original Boltzmann distribution that would require this for an exact calculation. The consequence is that the theory is limited to monovalent ions at room temperature in water, namely weak coupling regime (as showed in the aforementioned paper), for their correlations are smaller when compared to the correlations between ions of higher valences.

2.6 Numerical Solution of the PB Equation

The solution of the PB differential equation was achieved numerically via an iterative process. Therefore, it is convenient to rewrite the electrostatic potential in terms of the electric field $\boldsymbol{E}(r) = -\nabla\Phi(r)$, inserting this in Eq. (22) we get:

$$\nabla.\boldsymbol{E}(r) = \frac{4\pi}{\epsilon}\left[\sum_{i=1}^{N_m}\sigma_i\delta(r-r_i) - q\alpha\rho(r)\right] \tag{24}$$

By integrating the divergent of electric field, we find that the r component of the electric field $\boldsymbol{E}(r)$ satisfies an integral equation expression[27]:

$$\theta(x) = \frac{1}{x^2}\left[\sum_{i=1}^{N_m}\sigma_i - \alpha\chi(x)\right] \tag{25}$$

With $x = \frac{r}{\lambda_B}$, $\theta(x) = \beta q\lambda_B E(r)$,

$$\chi(x) = N_c\frac{\int_{\hat{a}+\hat{r_c}}^{x} dx'x'^2\, exp\left[-\alpha\int_{\hat{a}+\hat{r_c}}^{x'} dx''\theta(x'')\right]}{\int_{\hat{a}+\hat{r_c}}^{\hat{R}} dx'x'^2\, exp\left[-\alpha\int_{\hat{a}+\hat{r_c}}^{x'} dx''\theta(x'')\right]}\ , \tag{26}$$

where $\hat{a}+\hat{r}_c = (a+r_c)/\lambda_B$ and $\hat{R} = R/\lambda_B$.

The zero of the electrostatic potential $\Phi(R) = 0$ is taken at the cell boundary. The electric field inside the cell is calculated by an algorithm which

iterates Eq. (24) starting with an arbitrary function satisfying the boundary condition $E(R) = 0$ until it achieves convergence. The solution of the equation is important because it allows us to generate the density profiles of the counterions showed in the paper, this way we could better compare the theory to our computational simulations.

3. Final Considerations

Throughout this work we were able to obtain a range of different results in the form of density profiles, brush radii and the system's osmotic coefficients. The density profiles were able to illustrate that the difference in separation between the nanoparticle and the counterions, propelled by their repulsion to their images of equal charge, was not very significant when compared to the image free simulations. This is also true for the monomers and for the brush radius, with the exception of the trivalent counterion cases, when we can see a more relevant difference between both cases, which could be taken into consideration in the future for projects relying on a precise measurement of these parameters.

Utilizing a nanoparticle radius of $100\dot{A}$ and longer polymer chains, the divergence between the studied cases increases, This is expected from the point image charge equation $Q' = \gamma Qa/r_i$ since it is shown that the magnitude of this charge is directly proportional to the nanoparticle radius. This represents that the difference in cases could be further explored since we know that colloid particles typically range from $10\dot{A}$ to $10000\dot{A}$ in size, leaving us something to keep in mind for future works of this nature. The remaining results regarding the density profiles and the brush radius were as expected, the stronger bending of polymer chains in the multivalent counterion cases, resulting in a stronger confinement of those, and a smaller brush radius, have been studied previously[28-30]. These were in agreement with ours.

Finally, the mean-field PB theory presented here matched the results for the monovalent counterion cases, but it was not able to represent with precision the multivalent ion cases. This was expected as the PB theory is historically considered accurate for weak electrostatic couplings, for the reasons expressed in section 2.5, but poorly matched with cases where there are strong electrostatic couplings. The osmotic coefficients studied in regards to the system's volume fraction were the final results presented and they showed that increasing the polymer chain's length decreases the osmotic coefficients, which is in agreement with experimental measurements[31]. Physically this means that the absorption of counterions by the brush is inversely linked to the osmotic coefficient since the increase in polymer chain's length leads to increase in ion absorption. These last results also clarified that the decrease in nanoparticle curvature, represented by its increase in radius, would truly only affect the polarization effect if the volume fraction was not maintained constant in the process. However, similar volume fractions with a significant difference in nanoparticle radius could still show a considerable impact in the nanoparticle polarization.

4. Conclusion

During this work we took advantage of our previous knowledge in polymer sciences, acquired in my undergraduate thesis in polymer translocation, to fulfil a more complex work, this time with polyelectrolyte brushes. Initially we built a program that could simulate a neutral polymer brush where the only interactions between particles were the bond between monomers and a Lennard-Jones potential. Gradually, we added the electrostatic interactions, solving the computational problems that appeared along the way, we adapted the image potentials from my advisor previous works with colloids and we swapped the Lennard-Jones potential for a simpler hard spheres potential, for the reasons expressed in the paper. After this, we tested the program by comparing the results of the simulation conditions, without the polymers, to previous works of colloids immersed in electrolyte solutions. We then tested the complete brush against our PB theory for the brush (with a separate program for the theory calculations), concluding that the program was ready to obtain the simulation data for the work we planned.

The data was further analyzed by an algorithm that generated the density profiles and average brush radius, these were the main results for the discussion of the differences between the brush dynamics with and without consideration for the dielectric inhomogeneity. This discussion was the focus of the paper and our main objective, and in this we consider ourselves successful. The results obtained showed to which extent the polarization of the central nanoparticle in spherical PEBs can affect the equilibrium state of said brushes, which was shown to be small for most of the chosen parameters. However, further prospects can yet be achieved using the methods and modelling explained in the previous sections.

We found that the method chosen for the calculation of the polarization resulting of the dielectric difference from the central nanoparticle and its surrounding medium was an outstanding match for the work. The computational time added by the necessity of the image charge calculations was considerable, in reference to the image free cases it almost doubled. Nonetheless, the other methods for this purpose, which were mentioned in the paper, were shown to dawdle in comparison. Although the use of parallel programming was tried in the middle of the project, the calculations were not so numerous as to require its use, and because of this we ended-up only needing to use the C language, for a non-compilable language would not be optimized enough for the project.

For the prospects of the project we could cite the further exploration of the nanoparticle curvature and osmotic properties of the system in the polarizations studies. The current parameters of the simulation were chosen not only to match the experimental ones[32] but also to build a feasible modelling, a higher number of particles - something that could be used to better represent the polymer chains, the ionic solution, and allow a bigger

central particle – would result in higher simulations times. Higher simulation times make programming mistakes very costly, and they would undoubtedly happen being this the first time we perform a simulation of this type. Other possibilities of future work are in the use of a salt solution in addition to the ionic already present as to have a measure of the brush properties versus the solution concentration. The possibility of a moving brush or a shear flow is also being considerate because of the possibility of it better representing the brush dynamics inside the human body against blood flow, since one of the purpose of the synthetization of these brushes is as drug carriers.

Finally, the knowledge acquired throughout this project was enormous making it extremely compensating, not only for the opportunity to publish it, but for the treasured experience.

5. Acknowledgments

I would like to thank the Universidade Federal do Rio Grande do Sul for the support during my entire academic life, from the undergraduate physics course to the Masters degree, which allowed me to perform this work. The support of Alessanda Sarapio was also imperative in the makings of this project, she showed nothing but love and caring for me even when the stress was at its peak, she was my beacon of light. I thank also my advisor Alexandre for his ideas and knowledge shared, and for the valuable advising, present since my undergraduate thesis. I thank my family for the financial and emotional support during my entire life, specially my mother Rosa and my father Paulo. Finally. I would also like to thank the CNPq foundation for funding my Masters degree studies and supporting science in a country where being a scientist is unfortunately a daily struggle.

5. Agradecimentos

Eu gostaria de agradecer a Universidade Federal do Rio Grande do Sul pelo apoio durante toda a minha vida acadêmica, desde o curso de graduação em física até o mestrado, o que me permitiu concluir este trabalho. O apoio de Alessandra Sarapio também foi imperativo no desenvolvimento deste projeto, mesmo nos períodos de maior estresse ela mostrou nada além de amor a carinho por mim, ela foi o meu farol. Eu agradeço também o meu orientador Alexandre pelas ideias e conhecimentos a mim cedidos, e pelos aconselhamentos valiosos presentes desde a minha tese de conclusão da graduação. Eu agradeço à minha família pelo suporte financeiro e emocional durante toda a minha vida, especialmente à minha mãe Rosa e ao meu pai Paulo. Finalmente, eu também gostaria de agradecer ao Conselho Nacional de Desenvolvimento Científico e Tecnológico (CNPq) pelo apoio através de uma bolsa de mestrado, o que me permitiu desenvolver e concluir este projeto, e por apoiar a ciência em um país onde ser um cientista é infelizmente uma batalha diária.

6. References

1. V. B. Tergolina, A. P. dos Santos, J. Chem. Phys 147, 114103 (2017)
2. F. Buchholz, Trends Polym. 99, 277 (1992)
3. P. de Gennes, Scaling Concepts in Polymer Physics - Cornell University Press, Ithaca, NY, (1979)
4. J. Hayter, G. Janninck, F. Brochard-Wyart, and P. de Gennes, J. Phys - Paris Lett. 41, 451 (1980)
5. L. Wang, V. Bloomfield, Macromolecules 23, 804 (1990)
6. T. Witten, P. Pincus, Europhys. Lett. 3, 315 (1987)
7. K. Schmitz, Macroion Characterization: From Dilute Solutions to Complex Fluids, edited - American Chemical Society, Washington, DC, (1994)
8. M. Kim et al, Polymers, 7(7), 1346-1378 (2015)
9. M. Zhang, A. H. E. Muller, Journal of Polymer Science: Part A: Polymer Chemistry, Vol. 43, 3461–3481 (2005)
10. J. A. Jaber, J. B. Schlenoff, Current Opinion in Colloid & Interface Science 11, 324–329 (2006)
11. X. Huang, W. Liao, G. Zhang, S. Kang, C. Y. Zhang, Int J Nanomedicine; 12: 2215–2226 (2017)
12. A. P. dos Santos, A. Bakhshandeh, Y. Levin, J. Chem. Phys. 135, 044124 (2011)
13. W. T. Norris, IEE Proc. Sci., Meas. Technol. 142, 142 (1995).
14. R. Messina, J. Chem. Phys. 117, 11062 (2002)
15. G. I. Guerrero-Garcıa, M. O. de la Cruz, J. Phys. Chem. B 118, 8854 (2014)
16. V. Jadhao, F. J. Solis, M. O. de la Cruz, Phys. Rev. Lett. 109, 223905 (2012)
17. V. Jadhao, F. J. Solis, M. O. de la Cruz, J. Chem. Phys. 138, 054119 (2013)
18. De Gennes PG, Scaling Concepts in Polymer Physics (1979)
19. M. Quesada-Perez, A. Martın-Molina, Soft Matter 9, 7086 (2013).
20. J. C. Maxwell: 'A treatise on electricity and magnetism', Dover, reprinted 1954, 3rd edn. (1891)
21. J. Jeans: 'The mathematical theory of electricity and magnetism" Cambridge, 5th edn. (1948)
22. W. T. Norris, IEE Proc.: Sci., Meas. Technol. 142, 142 (1995)
23. A. P. dos Santos, A. Bakhshandeh, Y. Levin, J. Chem. Phys. 135, 044124 (2011)
24. W. F. van Gunsteren, H. J. C. Berendsen, Molec. Phys. 45 . 637 (1982)
25. M. G. Paterlini, D. M. Ferguson, Chemical Physics 236 243–252 (1998)
26. A. E. James, D. J. A. Williams, Journal of Colloid and Interface Science, Vol. 107, No. 1, September pg. 44 (1985)
27. Alexandre Diehl, Yan Levin, J. Phys. Condens. Matter 17 3309-3316 (2005)

28. P. Pincus, Macromolecules 24, 2912 (1991)
29. O. V. Borisov, T. M. Birshtein, E. B. Zhulina, J. Phys. II 1, 521 (1991)
30. Y. Mei, K. Lauterbach, M. Hoffmann, O. V. Borisov, M. Ballauff, A. Jusufi, Phys. Rev. Lett. 97, 158301 (2006)
31. B. Das, X. Guo, M. Ballauff, Prog. Colloid Polym. Sci. 121, 34 (2002)
32. M. Ballauff, Prog. Polym. Sci. 32, 1135–1151 (2007)